CHEMISTRY
A European Journal

A Journal of
ChemPubSoc Europe

Accepted Article

Title: Mesoporous MFI Zeolite with Two-Dimensional Square Structure Directed by Surfactants with Azobenzene Tail Group

Authors: Xuefeng Shen, Wenting Mao, Yanhang Ma, Honggen Peng, Dongdong Xu, Peng Wu, Lu Han, and Shunai Che

To be cited as: *Chem. Eur. J.* 10.1002/chem.201800307

Link to VoR: http://dx.doi.org/10.1002/chem.201800307

Supported by
ACES

WILEY-VCH

10.1002/chem.201800307

WILEY-VCH

Mesoporous MFI Zeolite with Two-Dimensional Square Structure Directed by Surfactants with Azobenzene Tail Group

Xuefeng Shen[+],[a] Wenting Mao[+],[a] Yanhang Ma,[b] Honggen Peng,[c] Dongdong Xu,[d] Peng Wu,[e] Lu Han*[a, f] and Shunai Che*[a, f]

+ These authors contributed equally to this work.

Abstract: Mesoporous MFI zeolites (MMZs) have been constructed by using the surfactant containing azobenzene segment in the hydrophobic tail. The cylindrical π-π stacking of azeobenzene groups is considered to be the key factor to form the ordered mesostructure through cooperative structural matching and the rearrangement of MFI frameworks. The mesostructure has been tuned from disordered hierarchical arrangement into an ordered two-dimensional (2D) square *p4mm* structure by changing the length of alkyl chain between diquaternary ammonium head group and azobenzene group. The geometrically matching between MFI zeolitic framework and the alkyl chain length plays an important role on the construction of the crystallographically correlated mesostructure with 2D-square ordering. A combination of X-ray diffraction patterns and electron microscopy studies provides visible evidence for the mesostructural transformation from short range hexagonal or lamellar ordering to 2D square mesostructure.

[a] X. Shen, W. Mao, Prof. L. Han, Prof. S. Che,
School of Chemistry and Chemical Engineering, State Key Laboratory of Metal Matrix Composites,
Shanghai Jiao Tong University,
800 Dongchuan Road, Shanghai, 200240 (P.R. China)
E-mail: chesa@sjtu.edu.cn, chesa@tongji.edu.cn, luhan@tongji.edu.cn

[b] Prof. Y. Ma,
School of Physical Science and Technology,
ShanghaiTech University,
100 Haike Road, Pudong, Shanghai, 201210 (P.R. China)

[c] Prof. H. Peng,
College of Chemistry,
Nanchang University,
999 Xuefu Road, Nanchang, Jiangxi, 330031 (P.R. China)

[d] Prof. D. Xu,
School of Chemistry and Mateirals Science, Jiangsu Key Laboratory of Biofunctional Materials,
Nanjing Normal University,
Nanjing, 210023 (P.R. China)

[e] Prof. P. Wu,
Shanghai Key Laboratory of Green Chemistry and Chemical Processes, School of Chemistry and Molecular Engineering,
East China Normal University,
3663 North Zhongshan Road, Shanghai, 200062 (P.R. China)

[f] Prof. L. Han, Prof. S. Che,
School of Chemical Science and Engineering,
Tongji University,
1239 Siping Road, Shanghai, China, 200092 (P. R. China)

Supporting information for this article is given via a link at the end of the document.

Introduction

Zeolites, microporous crystalline aluminosilicates, are widely used in the field of sorbents, ion-exchange, catalysts due to their high surface area and adsorption capacity, high thermal and hydrothermal stabilities, uniform and well-defined micropores with excellent shape-selectivity in catalysis.[1] The sole presence of micropores (mostly 0.4-1.2 nm) limits their applications in catalyzing organic molecules with large dimensions.[1a, 2] On the other hand, highly ordered mesoporous aluminosilicates with adjustable pore size from 1.5 to 15 nm and high surface areas opened a new possibility for preparing large molecule catalysts in the nanoporous space.[3] However, mesoporous aluminosilicates are disappointing for the actual catalysis process due to the amorphous wall that led to the poor hydrothermal stability and acidity. Synthesizing mesoporous zeolites could overcome these disadvantages. Until now, many synthesis methods have been reported, such as post-synthetic treatment of bulk zeolites,[4] assembly of zeolitic nanocrystals,[5] and hard or soft template methods.[6] Nevertheless, the direct synthesis of highly ordered mesoporous zeolites is still a challenge in material science that remains unresolved.

Quaternary ammonium salts have been widely used to generate zeolite structures due to their distinct kinetic size and steric configuration,[7] which lead to their close fit to inorganic framework.[8] To combine the templating units for both zeolite framework and the mesostructural ordering, Ryoo *et al.* designed a bifunctional surfactant and the lamellar mesostructured zeolites have been constructed by MFI nanosheets with three pentasil layer thickness.[9] Furthermore, a gemini-type, multiple quaternary ammoniums surfactant has been used to generate a hexagonally ordered mesoporous molecular sieves with MFI-like frameworks.[9c] In our previous

reports, we introduced aromatic groups into the hydrophobic tail of the surfactants,[10] the strong π-π interaction of which could stabilized the lamellar micelle structure, and the configuration of these aromatic could be adjusted to geometrically match the MFI zeolitic framework to form lamellar mesostructural MFI zeolites. The theoretical analysis indicates that the present of both multiple quaternary ammoniums and aromatic group could reduce binding energies of the mesostructured zeolite synthesis system.

It is well known that intergrowth is a common phenomenon in MFI zeolites, occasionally with the intergrowth with MEL-type structure.[11] The unit cell parameters of MFI along *a*- and *b*-axies (*a* = 20.07 Å, *b* = 19.92 Å) are almost the same, and both the straight channels and zig-zag channels of MFI zeolite are 10-membered ring (10-MR). These structure characteristic of MFI zeolite provide a fundamental possibility for an intergrowth relationship between the (*h*00) and (0*k*0) facets.[12] Bolaform or triply branched cationic surfactants were used to template mesostructured MFI zeolite constructed by MFI nanosheets joined with a 90° rotational boundary due to their special branched configuration and the stronger π-π stacking around the boundary joints.[10b,13] Tsapatsis et al. reported the hierarchical MFI zeolite with house-of-cards nanosheets with perpendicular arrangement that lead to 2 to 7 nm mesopores.[11b] Recently, we introduced an azobenzene segment into the hydrophobic tail of the amphiphilic surfactant, leading to the MFI zeolite with 2D square mesostructure framed by the intergrowth of MFI nanosheets expanding along the *a*-*c* plane.[14] The introduction of azobenzene segment in the hydrophobic part of surfactant could induce the cylindrical-assembly of surfactants, which could match the zeolite framework to form ordered mesoporous zeolites with 2D square mesostructure.

Herein, we investigate the formation mechanism of the MMZ templated by azobenzene-containing surfactants. To elucidate the importance of the length of alkyl chain and the templating effect with geometrical matching, the surfactants with different alkyl chain length connecting the diquaternary ammonium group and azobenzene segment were designed (Figure 1). These surfactants are donated as $C_{azo\text{-}m\text{-}6\text{-}6}$ (**m** denotes the length of the alkyl chain, the first **6** is the carbon chain connected two quaternary ammoniums and the second **6** is the carbon chain tail of the outer quaternary ammonium). The only difference of these surfactants is the length of the alkyl chain connecting azobenzene group and diquaternary ammonium group ($C_{azo\text{-}m\text{-}6\text{-}6}$, m= 6, 8, 10, 12). To understand the structural evolution of the MMZs and the molecular interaction during the synthesis, X-ray diffraction (XRD) patterns, scanning electron microscopy (SEM), transmission electron microscopy (TEM) studies and UV-Vis absorption spectroscopy of products with different reaction times were investigated.

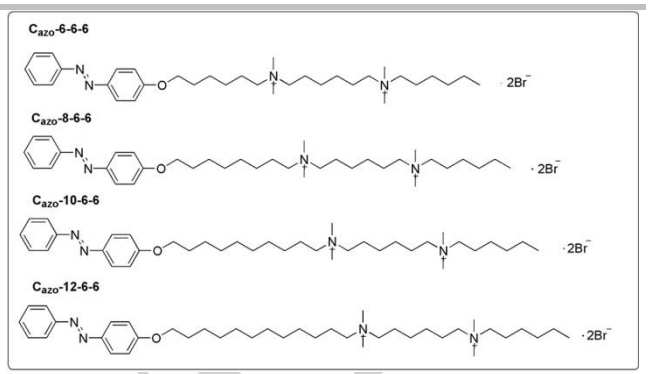

Figure 1. Chemical formulas of the surfactants with different carbon chain length.

Results and Discussion

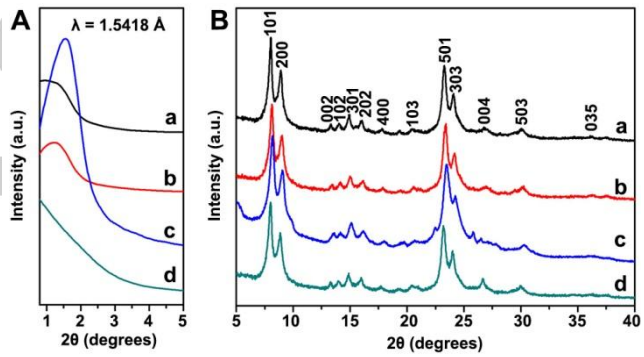

Figure 2. Low-angle (A) and high-angle (B) powder XRD patterns of calcined products MMZ-6 (a), MMZ-8 (b), MMZ-10 (c) and MMZ-12 (d) obtained by surfactants $C_{azo\text{-}6\text{-}6\text{-}6}$, $C_{azo\text{-}8\text{-}6\text{-}6}$, $C_{azo\text{-}10\text{-}6\text{-}6}$ and $C_{azo\text{-}12\text{-}6\text{-}6}$, respectively (wavelength 1.5418 Å).

Figure 2 shows the XRD patterns of calcined samples, namely MMZ-6, MMZ-8, MMZ-10 and MMZ-12 templated by $C_{azo\text{-}6\text{-}6\text{-}6}$, $C_{azo\text{-}8\text{-}6\text{-}6}$, $C_{azo\text{-}10\text{-}6\text{-}6}$ and $C_{azo\text{-}12\text{-}6\text{-}6}$, respectively. MMZ-6 shows one broad reflection in the low-angle region centred at 2θ = 1.2°, indicating the mesostructural ordering with the *d*-spacing of 7.4 nm. For MMZ-8, the reflection is more obvious with the same *d*-spacing. When the alkyl chain increased to C10, a well-resolved reflection at 2θ of 1.6° with the *d*-spacing of 5.6 nm can be recognized, suggesting the highly ordered mesostructure compared to MMZ-6 and MMZ-8. For the MMZ-12, the ordering of mesostructure decreased as nearly no reflection appears in the low-angle region. As revealed by the TEM observations (*vide post*), there is no clear correlation between the *d*-spacing of the mesostructure and the length of alkyl chain, which the reflections are mainly depending on the ordering of the structure. The high-angle XRD patterns (Figure 2B) indicate all these samples possess the MFI structure with

10.1002/chem.201800307

similar crystallinity and free of other phases. Most of the sharp peaks are associated with the *h*0*l* reflections of the MFI framework, which indicates the formation the layered MFI nanosheets expanding along the *ac* plane.

The SEM images are consistent with structural features discerned from their XRD patterns (Figure 3). All these samples show the house-of-cards morphology. MMZ-6 has the tetragonal shape with size of ~2 μm (Figure 3a_1), MFI nanosheets of which joined with rotational boundary (Figure 3a_2). These MFI nanosheets of MMZ-6 oriented growth along the central axis of tetragonal crystal, namely the *c*-axis of MFI framework (*vide post*). The diameter of MMZ-8 is smaller than MMZ-6 (Figure 3b_1). The intergrowth of MMZ-8 is sparser, and the thickness of nanosheets is much larger with some of the MFI nanosheets randomly stacked together (Figure 3b_2). There is no obviously oriented growth of the MFI nanosheets in MMZ-8 from the SEM images. The size of tetragonal particles of MMZ-10 is almost the same as MMZ-8 (~1.5 μm). MMZ-10 has the uniform morphology (Figure 3c_1) that a tetragonal shape with four curved surfaces meeting at the vertexes (Figure 3c_2). A four-fold order of rotation with the mirror planes inclined to each other by 45°, indicating the 4*mm* point group symmetry. There is no obvious MFI nanosheets viewed form the SEM images of MMZ-10, which is distinguished from other samples. Of note, the MFI nanosheets are ordered in the tetragonal particles with an oriented growth along the *c*-axis of MFI framework (*vide post*). MMZ-12 has a deformed rhombohedral morphology, the size of which is smaller than other three samples (Figure 3d_1). The intergrowth of MMZ-12 is not obvious, and the nanosheets of MMZ-12 is fragmentary with smaller size.

The TEM images observed on slice of the calcined MMZ samples embedded in epoxy resin show that all these materials have large amounts of mesopores framed by thin MFI nanosheets. The Fourier diffractograms (FDs) show that the intergrown perpendicular with each other, which is coincide with nanosheets expand in *ac* plane of MFI framework and he XRD patterns and SEM observations. Figure 4a_1 shows the low-magnification TEM image taken from the top view of the cross-section of MMZ-6. From the high-resolution TEM (HRTEM) image, it can be found the MFI nanosheets have the layered stacking of MFI nanosheets consist of 4-6 pentasils layers, which results in nonuniform mesopores with 1-2 pentasil layers thickness. This nonuniformity leads to the broad peak in the low-angle XRD profile. The diffusion of the diffraction spots in the FD shows the bending and frustration of the intergrowth structure. Figure 4b_1 shows the low-magnification TEM image of the cross-section of MMZ-8, indicating the sparse intergrowth structure with nonuniform layer thickness and disordered mesopores, which is also clearly shown in Figure 4b_2. Some MFI nanosheets collapsed after removal of surfactants due to the large void among the nanosheets. The diffusion of the diffraction spots in the FD pattern of MMZ-8 is more obvious due to the irregular intergrowth structure. It is worthy to note

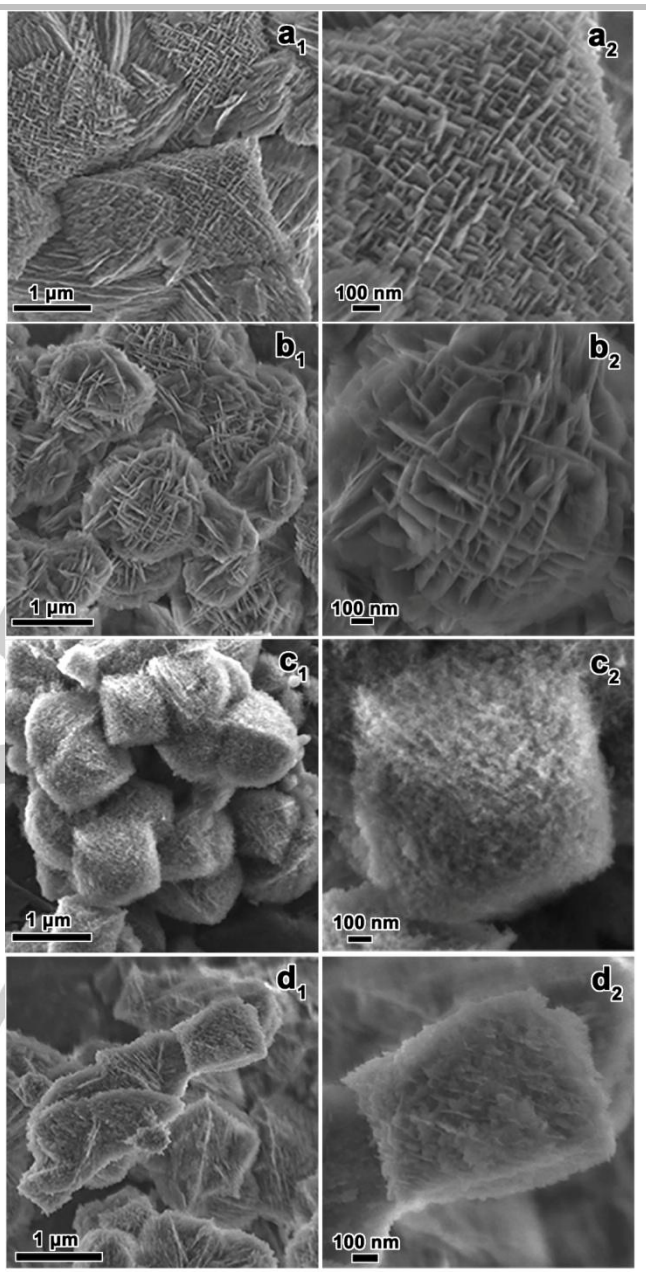

Figure 3. Low-angle (A) and high-angle (B) powder XRD patterns of calcined products MMZ-6 (a), MMZ-8 (b), MMZ-10 (c) and MMZ-12 (d) obtained by surfactants $C_{azo\text{-}6\text{-}6\text{-}6}$, $C_{azo\text{-}8\text{-}6\text{-}6}$, $C_{azo\text{-}10\text{-}6\text{-}6}$ and $C_{azo\text{-}12\text{-}6\text{-}6}$, respectively (wavelength 1.5418 Å).

that the ordered mesostructure can be only formed in MMZ-10, as shown in Figure4c. The cross-sectional image shown in Figure 4c_1 shows the tetragonal morphology. The ordered straight 2D square channels. framed by MFI nanosheets are observed in Figure 4c_2. The nanosheets consist of three pentasil layers and the pore diameter are uniform with three

10.1002/chem.201800307

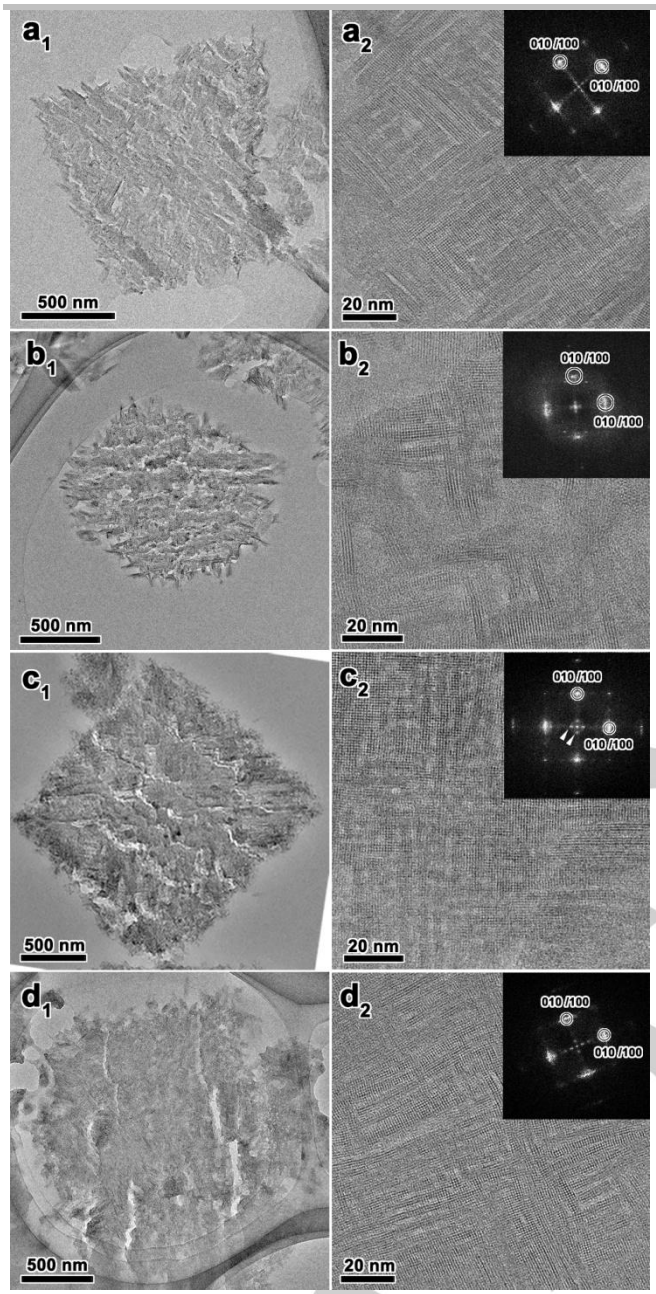

Figure 4. TEM images from the top view of the octahedron-like particles of the MMZ-6 (a), MMZ-8 (b), MMZ-10 (c) and MMZ-12 (d). The corresponding FDs were inserted in their HRTEM images. The white triangles indicate the diffraction spots of mesostructural ordering.

pentasil layers thickness. The rotational boundary of the joint MFI nanosheets is almost all 90°, connected with each with new Si-O-Si bonds between two related hydroxyl groups from *ac* and *bc* plane of MFI framework, respectively.[10a] A detailed structural study of MMZ-10 is shown in our previous publication.[14] The ordering of mesostructure of MMZ-10 resulted in the well-resolved peak in the low-angle XRD pattern. The ordering of mesostructure decreased when increasing the alkyl chain from C10 to C12. Figure 4d_1 shows the low-magnification TEM image of MMZ-12, showing the mesostructures framed by MFI nanosheets, however, with nonuniform thickness of the nanosheets with wide pore size distributions (Figure 4d_2).

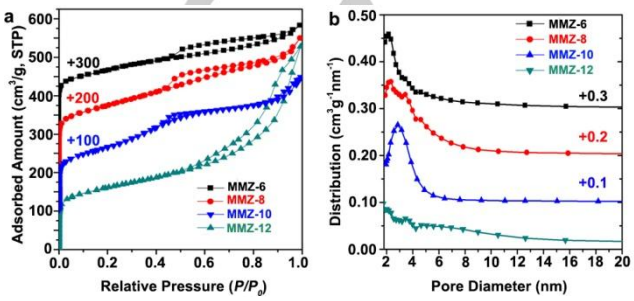

Figure 5. N_2 adsorption-desorption isotherms (a) and pore size distribution curves (b) obtained from desorption branches of calcined mesoporous zeolites shown in Figure 2.

Table 1. The pore properties of calcined MMZ-6, MMZ-8, MMZ-10 and MMZ-12.

Samples	S_{BET}[a] (m^2 g^{-1})	V_{Micro}[b] (cm^3 g^{-1})	V_{Total}[c] (cm^3 g^{-1})
MMZ-6	551	0.16	0.44
MMZ-8	595	0.17	0.54
MMZ-10	604	0.16	0.53
MMZ-12	540	0.12	0.80

[a] BET surface area calculated from the adsorption data obtained at P/P_0 between 0.05 and 0.25. [b] Micropore volume determined via the *t*-plot method. [c] Total pore volume determined via the single-point method.

The N_2 adsorption-desorption data of the samples are shown in Figure 5a. All samples show the existence of micropores, as evidenced by a sharp increasing adsorption capacity at P/P_0 < 0.02. The calcined MMZ-6, MMZ-8 and MMZ-10 exhibit type-IV isotherms with H4-type hysteresis loop.[15] The hysteresis loops of MMZ-6 and MMZ-8 at relative pressures in the range of P/P_0 = 0.5-0.9 indicate the mesopores with wide pore size distributions. Compared with MMZ-6 and MMZ-8, MMZ-10 shows a higher uptake and the hysteresis loop in the range of P/P_0 = 0.4-0.6 indicates the presence of abundant uniform mesopores. The N_2 adsorption-desorption isotherms of MMZ-12 exhibit a type-IV isotherm and a H3-type hysteresis loop, which shows this sample has disordered lamellar or slit pores. The pore size distribution of the samples obtained from adsorption

branches are shown in Figure 5b, the MMZ-6 shows mesopore diameter of ~2.2 nm, which is agree with the HRTEM observations. The MMZ-8 shows a wide pore size distribution, indicating the nonuniform mesopores in the structure. The MMZ-10 shows the uniform mesopores with pore size of ~3 nm. The MMZ-12 shows no obvious pore size distribution peaks, indicating the nonuniform mesopores. All the samples exhibit BET surface area larger than 500 $m^2 g^{-1}$ (Table 1). MMZ-10 has the highest BET surface area among these four materials dues to the ordered mesostructure. The MMZ-12 has the highest mesopore volume, suggesting the existence of large mesopores due to the nonuniform stacking of the MFI nanosheets.

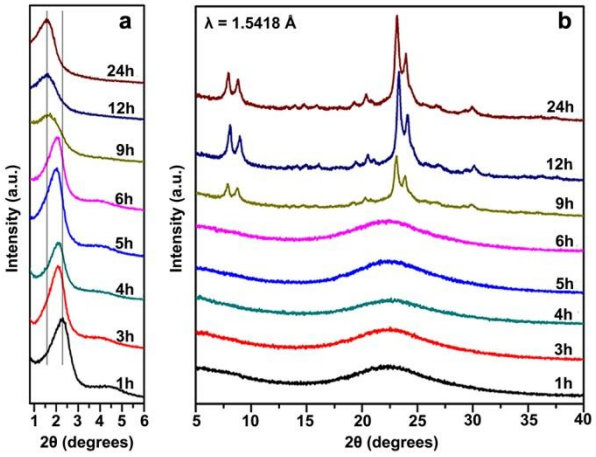

Figure 6. Low-angle (a) and high-angle (b) powder XRD patterns of as-synthesized products obtained by surfactant $C_{azo\text{-}10\text{-}6\text{-}6}$ for various crystallization time at 423 K.

The morphological and structural evolution of MMZ-10. To investigate the morphological and structural evolution of MMZ-10, the crystallization process of MMZ-10 was investigated as a function of reaction time. After being mixed at 333 K with vigorous magnetic stirring for 3 h, the original silica gel was evenly divided into identical Teflon-lined stainless-steel autoclaves, and the zeolite powder was collected after different crystallization periods (1 h-24 h). Figure 6 shows the low- and high-angle powder XRD patterns of the products collected during the crystallization periods. The low-angle XRD pattern of the products before 6 h shows a strong reflection with a 2θ of 2.3° and a broad second-order reflection centred at 4.5°. The two reflections with a *d*-spacing ratio of 2 : 1 probably indicate the formation of lamellar mesostructures. However, other 2D- and 3D- mesostructures cannot be excluded. No reflections were detected in the high-angle region before 6h. As the product crystallized for 9 h, the first-order reflection at a 2θ of 2.3° shifted to a lower angle, while the second-order reflection disappeared, suggesting a structural rearrangement or transformation. Simultaneously, high-angle reflections corresponding to the MFI zeolite structure appeared. As the product crystallized to 24 h, the first-order reflection shifted to a 2θ of 1.59°, which is same to the final product (4 days) with a d-spacing of 5.6 nm, and the high-angle reflections became stronger, suggesting an improved mesostructured ordering and an increased crystallinity. A crystallization period of 24 h under the present synthesis conditions is sufficient for the complete transformation from an amorphous aluminosilicate framework to MFI zeolite with 2D square mesostructure. Further hydrothermal treatment (*e.g.*, 4 days) did not result in significant changes in the mesostructure, which only increases the zeolitic crystallinity.

The structural transformation of the products was observed in SEM images (Figure 7). At the initial stage of crystallization (1-3 h), an undefined morphology was observed, which was probably amorphous aluminosilicate aggregates. The initial tetragonal morphology was first observed at 4 h with a particle size of ~300 nm. As the crystal morphology is commensurate with the structure, the appearance of the tetragonal morphology indicates the beginning of the crystallization process at atomistic scale. More tetragonal particles with a size of 400 nm formed at 6 h, but still there is much amorphous aluminosilicate aggregates, which results in no high-angle reflections corresponding to the MFI zeolite structure in the high-angle XRD pattern. Prolonging the crystallization process to 9 h, almost no amorphous aluminosilicate aggregates existed, the high-angle XRD pattern of which showed reflections of MFI framework. Finally, uniform tetragonal particles were formed at 24 h upon the completion of the silica condensation and crystallization. It is worthy to note that the average particle size of the final product was ~1.5 μm, which is same as the final product after 4 days, suggesting the sample grew from the initially formed particles and almost no significant changes of morphology from 24h.

Representative TEM images (Figure 8) of the products obtained at different crystallization period distinctly illustrated the transformation process from the amorphous aluminosilicate to crystalline zeolite. The selected-area electron diffraction (SAED) pattern of the samples crystallized for 1-3 h shows a ring pattern corresponding to a uniform *d*-spacing of ~4 nm, and the HRTEM images of the sample in this stage show the contrast of disordered mesostructures (Figure 8a). No crystalline phase or lamellar structure was observed at this stage, which the HRTEM and the corresponding FD are consistent with this result. Therefore, the low-angle reflections observed in the XRD pattern may not be the lamellar phase but rather due to the disordered packing of the micelles of uniform size. The micelles can be cylindrical, and the assemblies of the micelles may have short range hexagonally or lamellar ordering, which were marked by circles and rectangle. A particle with an early tetragonal morphology was discovered at approximately 4 h (Figure 8b). The weak diffraction spots in the SAED pattern suggest the appearance of atomistic crystalline structure. The HRTEM shows partially crystallized lattice fringes with a sheet-

10.1002/chem.201800307

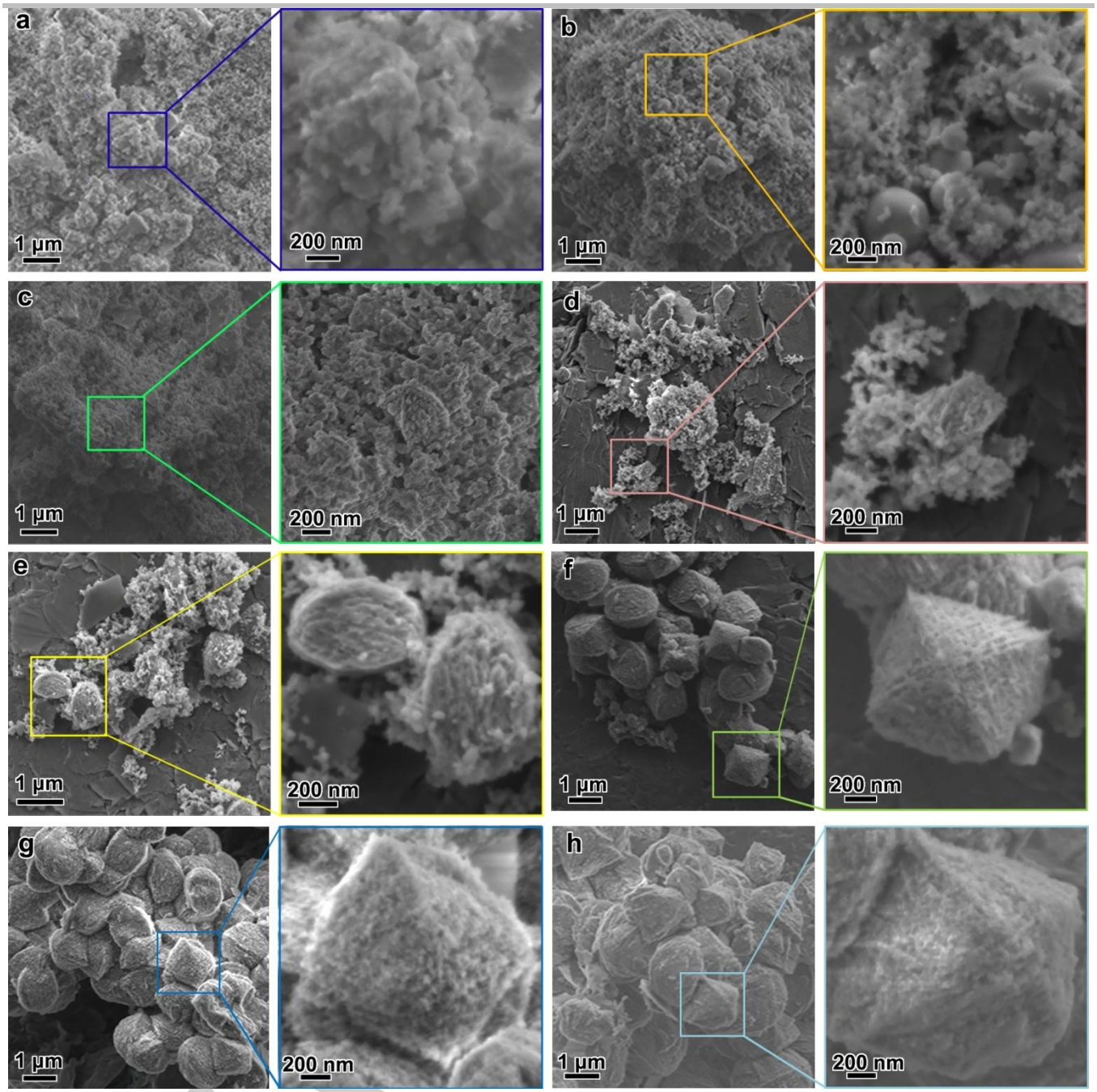

Figure 7. Representative SEM images of the as-synthesized products obtained by surfactant $C_{azo\text{-}10\text{-}6\text{-}6}$ for various crystallization times at 423 K for 1 h (a), 3 h (b), 4 h (c), 5 h (d), 6 h (e), 9 h (f), 12 h (g), 24 h (h).

like arrangement along one direction while the other part of the particle remains disordered, indicating the coexistence of amorphous silica and crystals, and the FD in the HRTEM shows the same diffraction pattern. Then, the SAED pattern taken from the sample crystallized for 5 h shows that the diffraction spots of the MFI crystal become clearer as the crystallization continues (Figure 8c). The TEM image shows enlarged particles with a tetragonal morphology and the HRTEM shows crystalline nanosheets in 90° rotation

WILEY-VCH
10.1002/chem.201800307

orientations. At 6 h, the SAED pattern shows the four-fold mesostructural ordering (indicated by white triangles) with the highly crystallized MFI lattice (Figure 8d). The HRTEM image taken from the cross-sections of tetragonal particles indicates the much higher crystallinity of the zeolite structure and good consistency with the structural matching of the 2D-square mesostructures with 90° rotational boundaries. The FD pattern shows more clear diffraction spots of MFI framework.

UV-vis spectroscopy was used to investigate the stereoregularity of $C_{azo\text{-}10\text{-}6\text{-}6}$ molecules (Figure 9). The UV-Vis absorption spectra of template molecules ($C_{azo\text{-}10\text{-}6\text{-}6}$) in dilute water clearly show two absorption bands, which are ascribed to the π in transition (348 nm) and the n-π transition (440 nm) of the azobenzene moieties,[16] respectively. The UV-Vis absorption spectra of all as-synthesized products obtained after different crystallization periods (1 h - 24 h) show three characteristic bands at 348, 376 and 440 nm. The increasing intensity of absorption bands at 376 nm and 440 nm during this crystallization period is due to the close and regular packing of the surfactants, which led to obvious π-π interactions between the azobenzene groups. Then the corresponding absorption bands shifted toward longer wavelengths (red-shift). The appearance of a new absorption band at 376 nm is due to the π-π interaction, which shift approximately 28 nm compared to the pure surfactant in dilute water (from 348 nm to 376 nm). Therefore, the azobenzene group of the surfactant is *trans*-form and kept intact in the whole present synthetic process.

From the above results, a mechanism is proposed based on the organic-inorganic interaction and the structural transition by geometrical matching mechanism. (i) Mesostructure formation. When the silica source is added to the surfactant solution, the quaternary ammonium sites of the surfactant interact with the silica species through electrostatic force and π-π interactions in the hydrophobic part. The self-assembly of the surfactant/silica species forms a cylindrically assembled mesostructure in a cooperative manner. Some of short range hexagonally or lamellar ordering was generated. The short range of these ordering may resulted in two reflections with a *d*-spacing ratio of 2 : 1 were appeared in the low-angle XRD patterns of the products sampled before 3 h. At this stage of the reaction, the framework is amorphous aluminosilicate, as shown in the XRD patterns. (ii) Nucleation and crystallization. With the ageing process, the quaternary ammonium groups pendant on the azobenzene lead to the gradual formation of crystalline zeolite frameworks[1c,17] (4 h). The nucleation and crystal growth at the beginning might be homogeneous, so the initially formed morphology is isotropic. (iii) Cooperative structural matching and rearrangement. With further ageing, one growth direction becomes dominant in the particles. As the structure of the MFI crystal and the possible MFI nanosheets are connected to each other with a 90° rotational angle, the MFI crystal grew gradually with an intersectional *a*/*b*-axis and a unique common *c*-axis, leading to the elongated tetragonal morphology. The pre-formed disordered mesostructure was rearranged and transformed into the cylindrical assembly-units to match the mesostructural ordering and the MFI sheet, forming the new 2D-square lattice. This process is consistent with the shift and the decrease in intensity of the low-angle XRD and the appearance of the high-angle reflections (6-9 h). (iv) Further crystallization and growth.

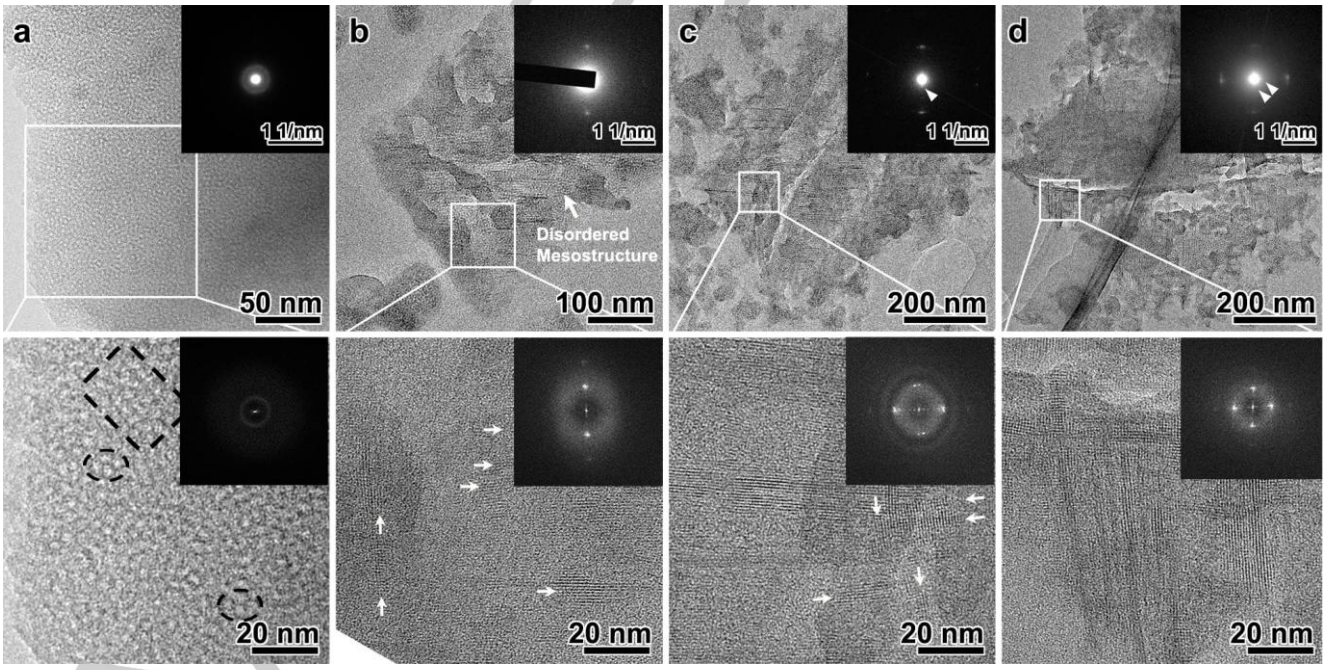

Figure 8. Representative TEM images of the as-synthesized products obtained at 423 K with various crystallization times of 3 h (a), 4 h (b), 5 h (c) and 6 h (d). The SAED patterns and FDs were inserted in the corresponding TEM and HRTEM images, respectively.

WILEY-VCH
10.1002/chem.201800307

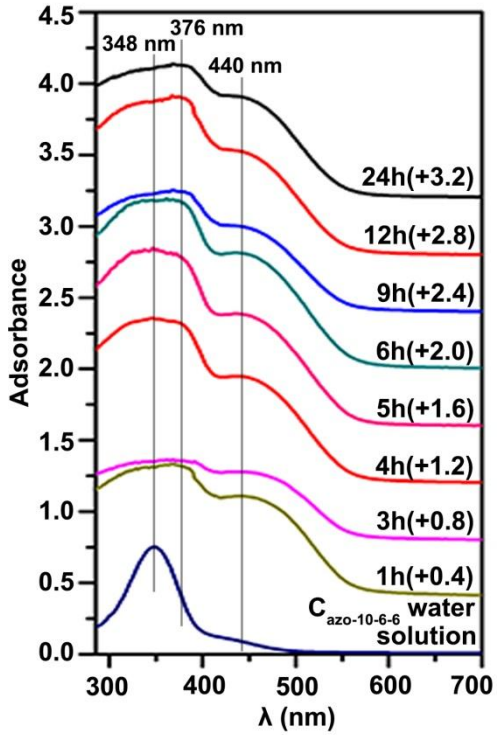

Figure 9. Representative UV-vis spectra of the as-synthesized products for various crystallization times at 423K.

Finally, the products were formed as a result of the crystallization process and the crystal growth (> 9 h). As the MFI growth along the *c*-axis direction perpendicular to the *a*-*b* plane is independent, which lead the final product to show a typical tetragonal morphology with an elongated shape.

Based on the experimental results and the discussions above, it can be considered that the mesostructure was formed by the cylindrical-assembly-units and the structural matching between the mesostructure and zeolite are the key factors for the synthesis of ordered MMZ. Among the four surfactants, highly ordered MMZ can be only formed by $C_{azo\text{-}10\text{-}6\text{-}6}$, while other surfactants only gave random intergrowth structures. It can be concluded that the alkyl chain length of the surfactant plays an important role in the mesostructure formation. This can be explained in terms of geometric matching between the assembly-units and MFI frameworks. In the intergrowth MFI zeolite, the (100) plane overgrown on the (010) plane due to the similar unit cell parameters of MFI along *a*- and *b*-axis (a = 20.07 Å, b = 19.92 Å) and both 10-MR pores of straight channels and zig-zag channels of MFI zeolite.[11,12] The *d*-spacing of 2D square MFI mesostructure is 5.9 nm (Figure S1a), and the corresponding mesopore with three pentasil layers space is ~3 nm. To direct this 2D square MFI mesostructure, these azobenzene-containing surfactants would be assembled into a square columnar packing, which is very rare to generated due to the long-range ordering is always formed by maximizing the interaction energy and minimizing the excluded volume.[18] However, in a few cases, the 2D square packing have been found in the liquid crystal phases by T-shape molecules[19] and in DNA condensed phases.[20]

It has been reported that achiral or chiral compounds bearing a relatively bulky head group and a hydrocarbon tail can be organized into chiral supramolecular assemblies by spontaneous symmetry breaking. The trans-azobenzene unit has a planar molecular configuration, which favours the cooperative packing in a helical sense due to the strong intermolecular interactions facilitated by the π-π stacking interactions and the steric hindrance triggered by the overcrowded alignment of the adjacent bulky headgroups (diquaternary ammoniums in azobenzene-containing surfactant).[21] The azobenzene-containing compounds tend to assemble into a helical sense due to the characteristic of the azobenzene segment. Therefore, a helix cylindroid micelle with 12 surfactant molecules in one pitch can be expected (Figure S1a).[14] The 12 terminal quaternary ammoniums would direct 12 straight channels surrounding the helical azobenzene cylinder to form the 2D square intergrown MFI frameworks (Figure S1b),[14] and other 12 quaternary ammoniums are at the pore opening of the 10-MR to stabilize the (010) surface. The diameter of the central cylinder is ~1.6 nm. The quaternary ammoniums tethered on the azobenzene with different largest length of ~0.7 nm ($C_{azo\text{-}6\text{-}6\text{-}6}$), ~1.0 nm ($C_{azo\text{-}8\text{-}6\text{-}6}$), ~1.2 nm ($C_{azo\text{-}10\text{-}6\text{-}6}$) and ~1.5 nm ($C_{azo\text{-}12\text{-}6\text{-}6}$) (Figure S1b). The π-π stacking of azobenzene segments not only exists between the adjacent azobenzenes in one circle but also those in adjacent azobenzenes in adjacent circles, which could effectively stabilize the helical structure.[14]

On the detailed calculation of the square mesopores with three pentasil layers space, the space from the azobenzene segment to the framework needs to be in a range of 0.8-1.3 nm considering the shortest length to reach the framework perpendicularly and longest distance through the diagnal, (Figure S1b). Due to the apporoprate chain length of $C_{azo\text{-}10\text{-}6\text{-}6}$ (~1.2 nm) and its flexiblility, its configuration can be adjusted to fit the requirement of the square mesopore (Figure S1b and e). Nevertheless, the chain length of $C_{azo\text{-}6\text{-}6\text{-}6}$ (~0.7 nm) (Figure S1c) and $C_{azo\text{-}8\text{-}6\text{-}6}$ (~1.0 nm) (Figure S1d), are too short while that of $C_{azo\text{-}12\text{-}6\text{-}6}$ (~1.5 nm) (Figure S1f) is too long to fit the structural intergrowth. Thus, the strict geometrical matching is essential for the ordered mesostructural formation.

Conclusions

By incorporating an azobenzene segment into the hydrophobic tail of the diquaternary ammonium surfactant, hierarchical MFI zeolite with 2D square mesostructure was successfully synthesized. Compared to the conventional cationic surfactants, the presence of azobenzene not only provided π-π stacking interactions to stabilize the micelles of surfactants, but also formed the cylindrical-assembly-units to match with the MFI zeolite framework. By controlling the alkyl chain length, the geometrical matching between cylindrical micelles and MFI framework gave rise to ordered arrangement of alternating MFI

WILEY-VCH
10.1002/chem.201800307

nanosheets through a mesostructural transformation and the crystallization process afterwards. We hole our findings will open up new possibilities for the elaborate fabrication of three-dimensionally ordered mesoporous zeolites.

Experimental Section

Synthesis of azobenzene-containing surfactants: 4.0 g (20 mmol) 4-Phenylazophenol was dissolved in 200 ml of ethanol under nitrogen atmosphere, then 1.2 g (22 mmol) potassium hydroxide and 30 g 1,10-dibromodecane (100 mmol) were added into the solution. Refluxing under 353 K for 20 hours, $C_{azo\text{-}10}$ was obtained by filter and washed by deionized water and anhydrous ethanol after the reaction system fully cooled. 8.4 g (20 mmol) $C_{azo\text{-}10}$ and 17.2 g (100 mmol) *N*,*N*,*N*',*N*'-Tetramethyl-1,6-hexanediamine was dissolved in 200 ml of acetonitrile and toluene mixed solution and refluxed at 357 K for 20 hours. After cooling to room temperature, solvent was removed by evaporation and then the product was filtered, washed with diethyl ether, and dried in a vacuum. 11.8 g (20 mmol) $C_{azo\text{-}10\text{-}6}$ and 9.9 g (60 mmol) 1-bromohexane were dissolved in 200 ml of acetonitrile and refluxed for 20 hours. After evaporation to remove acetonitrile, the product was filtered, washed with diethyl ether, and dried in a vacuum to obtain $C_{azo\text{-}10\text{-}6\text{-}6}$ as a yellow solid. The synthetic method of other surfactants ($C_{azo\text{-}m\text{-}6\text{-}6}$, m= 6, 8, 12) is almost the same as $C_{azo\text{-}10\text{-}6\text{-}6}$.

Synthesis of MMZ: The $C_{azo\text{-}m\text{-}6\text{-}6}$ surfactant was obtained in the form of $C_{azo\text{-}m\text{-}6\text{-}6}2Br$. In a typical synthesis, the surfactant, sodium aluminate, NaOH, and distilled water were mixed together and stirred at 333K for approximately 0.5 h. Tetraethyl orthosilicate was added to yield a molar composition of 1 $C_{azo\text{-}10\text{-}6\text{-}6}$: 25 SiO_2: 6.3 Na_2O: 0.3 Al_2O_3: 2000 H_2O, and the mixtures were stirred for an additional 3 h at 333K. The crystallisation process was conducted in Teflon-lined stainless steel autoclaves at 423 K, with the autoclaves tumbling at 40 rpm. The zeolite product was filtered, washed with distilled water and dried at 353 K overnight, and then they were calcined in air at 823 K. The mesoporous MFI zeolites (MMZ) templated by $C_{azo\text{-}6\text{-}6\text{-}6}$, $C_{azo\text{-}8\text{-}6\text{-}6}$, $C_{azo\text{-}10\text{-}6\text{-}6}$ and $C_{azo\text{-}12\text{-}6\text{-}6}$ were donated as MMZ-6, MMZ-8, MMZ-10 and MMZ-12, respectively.

Characterization: Powder XRD patterns were recorded on a Rigaku X-ray diffractometer D/max-IIIA equipped with a Cu K_α radiation source (40 kV, 30 mA). SEM was conducted on JEOL JSM-7401F operating at 1 kV and a JEOL JSM-7800F operating at 2 kV. HRTEM was performed using JEOL JEM-2100Lab$_6$ operating at 200 kV (Cs = 1.0 mm, point resolution of 2.3 Å). Images were recorded with a Keen View CCD camera (resolution of 1376 pixels × 1032 pixels, pixel size of 6.45 μm × 6.45 μm) at 50000−120000× magnification under low-dose conditions. The nitrogen adsorption/desorption isotherms were measured at 77 K using an ASAP 2010 M+C analyser. ^{1}H Nuclear Magnetic Resonance (NMR) spectra were recorded on a Varian MERCURY plus-400 (400 MHz) spectrometer, and the chemical shifts are reported in ppm relative to the residual deuterated solvent and the internal standard tetramethylsilane.

Acknowledgements

This work was supported by the National Natural Science Foundation of China (21533002, 21471099, 21571128), the National Key R&D Program of China (2016YFC0205900), the National Excellent Doctoral Dissertation of PR China (201454) and Shanghai Rising-Star Program (17QA1401700).

Keywords: Mesoporous zeolite • MFI zeolite • Surfactant self-assembly • Azobenzene group • Geometrical matching

[1] a) A. Corma, *Chem. Rev.* **1997***, 97*, 2373-2420; b) C. S. Cundy, P. A. Cox, *Chem. Rev.* **2003***, 103*, 663-702; c) M. E. Davis, R. F. Lobo, *Chem. Mater.* **1992**, *4*, 756-768.

[2] a) Y. Tao, H. Kanoh, L. Abrams, K. Kaneko, *Chem. Rev.* **2006**, *106*, 896-910; b) C. M. A. Parlett, K. Wilson, A. F. Lee, *Chem. Soc. Rev.* **2013**, *42*, 3876-3893; c) C. Perego, R. Millini, *Chem. Soc. Rev.* **2013**, *42*, 3956-3976; d) S. Van Donk, J. H. Bitter, A. Verberckmoes, M. Versluijs-Helder, A. Broersma, K. P. de Jong, *Angew. Chem. Inter. Ed.* **2005**, *44*, 1360-1363.

[3] a) C. T. Kresge, M. E. Leonowicz, W. J. Roth, J. C. Vartuli, J. S. Beck, *Nature* **1992**, *359*, 710-712; b) J. S. Beck, J. C. W. J. Vartuli, Roth, M. E. Leonowicz, C. T. Kresge, K. D. Schmitt, C. T. W. Chu, D. H. Olson, E. W. Sheppard, S. B. McCullen, J. B. Higgins, J. L. Schlenker, *J. Am. Chem. Soc.* **1992**, *114*, 10834-10843.

[4] a) J. C. Groen, T. Bach, U. Ziese, A. M. Paulaime-van Donk, K. P. de Jong, J. A. Moulijn, J. Pérez-Ramírez, *J. Am. Chem. Soc.* **2005**, *127*, 10792-10793; b) A. H. Janssen, A. J. Koster, K. P. de Jong, *Angew. Chem.* **2001**, *113*, 1136-1138.

[5] a) M. W. Anderson, S. M. Holmes, N. Hanif, C. S. Cundy, *Angew. Chem.* **2000**, *112*, 2819-2822; b) M. Choi, K. Na, J. Kim, Y. Sakamoto, O. Terasaki, R. Ryoo, *Chem. Commun.* **2009**, *20*, 2845-2847; c) K. Möller, B. Yilmaz, R. M. Jacubinas, U. Müller, T. Bein, *J. Am. Chem. Soc.* **2011**, *133*, 5284-5295; d) W. Chaikittisilp, Y. Suzuki, R. R. Mukti, T. Suzuki, K. Sugita, K. Itabashi, A. Shimojima, T. Okubo, *Angew. Chem. Int. Ed.* **2013**, *125*, 3439-3443; e) S. P. B. Kremer, C. E. A. Kirschhock, A. Aerts, K. Villani, J. A. Martens, O. I. Lebedev, G. Van Tendeloo, *Adv. Mater.* **2003**, *15*, 1705-1707; f) S. P. B. Kremer, C. E. A. Kirschhock, M. Tielen, F. Collignon, P. J. Grobet, P. A. Jacobs, J. A. Martens, *Adv. Funct. Mater.* **2002**, *12*, 286-292.

[6] a) H. S. Cho, R. Ryoo, *Microporous Mesoporous Mater*. **2012**, *151*, 107-112; b) W. Fan, M. A. Snyder, S. Kumar, P.-S. Lee, W. C. Yoo, A. V. McCormick, R. L. Penn, A. Stein, M. Tsapatsis, *Nat. Mater.* **2008**, *7*, 984-991; c) J. Wang, M. Yang, W. Shang, X. Su, Q. Hao, H. Chen, X, Mao, *Microporous Mesoporous Mater.* **2017**, *252*, 10-16; d) C. J. H. Jacobsen, C. Madsen, J. Houzvicka, I. Schmidt, A. Carlsson, *J. Am. Chem. Soc.* **2000**, *122*, 7116-7117; e) M. Choi, H. S. Cho, R. Srivastava, C. Venkatesan, D. H. Choi, R. Ryoo, *Nat. Mater.* **2006**, *5*, 718-723; f) H. Wang, T. J. Pinnavaia, *Angew. Chem. Int. Ed.* **2006**, *45*, 7603-7606; g) F. Liu, T. Willhammar, L. Wang, L. Zhu, Q. Sun, X. Meng, W. Carrillo-Cabrera, X. Zou, F. Xiao, *J. Am. Chem. Soc.* **2012**, *134*, 4557-4560. h) M. Khaleel, A. J. Wagner, K. A. Mkhoyan, M. Tsapatsis, *Angew. Chem. Int. Ed*. **2014**, *53*, 9456-9461; i) A. Inayat, I. Knoke, E. Spiecker, W. Schwieger, *Angew. Chem. Int. Ed.* **2012**, *51*, 1962-1965.

[7] a) S. L. Burkett, M. E. Davis, *J. Phys. Chem.* **1994**, *98*, 4647-4653; b) C. E. A. Kirschhock, R. Ravishankar, F. Verspeurt, P. J. Grobet, P. A. Jacobs, J. A. Martens, *J. Phys. Chem. B* **1999**, *103*, 4965-4971.

[8] a) R. M. Barrer, Academic Press London **1982**, Vol. 15; b) E. M. Flanigen, J. M. Bennett, R. W. Grose, J. P. Cohen, R. L. Patton, R. M. Kirchner, J. V. Smith, *Nature* **1978**, *271*, 512-516; c) B. Lok,; T. R. Cannan, C. Messina, *Zeolites* **1983**, *3*, 282-291.

[9] a) M. Choi, K. Na, J. Kim, Y. Sakamoto, O. Terasaki, R. Ryoo, *Nature* **2009**, *461*, 246-249; b) K. Na, M. Choi, W. Park, Y. Sakamoto, O. Terasaki, R. Ryoo, *J. Am. Chem. Soc.* **2010**, *132*, 4169-4177; c) K. Na, C. Jo, J. Kim, K. Cho, J. Jung, Y. Seo, R. J. Messinger, B. F. Chmelka, R. Ryoo, *Science* **2011**, *333*, 328-332.

[10] a) D. Xu, Y. Ma, Z. Jing, L. Han, B. Singh, J. Feng, X. Shen, F. Cao, P. Oleynikov, H. Sun, O. Terasaki, S. Che, *Nat. Commun.* **2014**, *5*, 4262; b) D. Xu, Z. Jing, F. Cao,; H. Sun, S. Che, *Chem. Mater.* **2014**, *26,* 4612-4619.

[11] a) N. A. Ramsahye, B. Slater, *Chem. Commun.* **2006**, 442-444; b) X. Zhang, D. Liu, D. Xu, S. Asahina, K. A. Cychosz, K. V. Agrawal, Y. Al

WILEY-VCH
10.1002/chem.201800307

Wahedi, A. Bhan, S. Al Hashimi, O. Terasaki, M. Thommes, M. Tsapatsis, *Science* **2012**, *336*, 1684-1687; c) T. Ohsuna, O. Terasaki,; Y. Nakagawa, S. I. Zones, K. Hiraga, *J. Phys. Chem. B* **1997**, *101*, 9881-9885; d) W. Chaikittisilp,; Y. Suzuki, R. R. Mukti, T. Suzuki, K. Sugita, K. Itabashi, A. Shimojima, T. Okubo, *Angew. Chem. Int. Ed.* **2013**, *52*, 3355-3359.

[12] G. T. Kokotailo, S. L. Lawton, D. H. Olson, W. M. Meier, *Nature* **1978**, *272*, 437-438.

[13] J. Čejka, S. *Catal. Rev.* **2007**, *49*, 457-509.

[14] X. Shen, W. Mao, Y. Ma, D. Xu, P. Wu, O. Terasaki, L. Han, S. Che, *Angew. Chem. Int. Ed.* **2017**, *57*, 724-728.

[15] a) R. Pierotti, J. Rouquerol, *Pure Appl. Chem.* **1985**, *57*, 603-619; b) J. Shen, L. Xu, Y. Liu, C. Lu, W. Hou, J. Zhu, *Chem. Mater.* **2008**, *20*, 3034-3041; c) N. Katcho, E. Urones-Garrote, D. Ávila-Brande, A. Gómez-Herrero, S. Urbonaite, S. Csillag, E. Lomba, F. Agulló-Rueda, A. R. Landa-Cánovas, L. C. Otero-Díaz, *Chem. mater.* **2007**, *19*, 2304-2309.

[16] A. A. Beharry, G. A. Woolley, *Chem. Soc. Rev.* **2011**, *40*, 4422-4437.

[17] S. L. Burkett, M. E. Davis, *Chem. Mater.* **1995**, *7*, 920-928.

[18] R. Hołyst, P. Oswald, Macromol. *Theory Simul.* **2001***, 10*, 1–16.

[19] a) B. Chen, X. Zeng, U. Baumeister, G. Ungar, C. Tschierske, *Science* **2005**, *307*, 96–99; b) B. Chen, U. Baumeister, S. Diele, M. Das, X. Zeng, G. Ungar, C. Tschierske, *J. Am. Chem. Soc.* **2004**, *126*, 8608–8609.

[20] C. Jin, L. Han, S. Che, *Angew. Chem. Int. Ed.* **2009***, 48*, 9268–9272; b) L. Han, C.Jin, B. Liu, S. Che, *Chem. Mater.* **2012***, 24*, 504–511.

[21] a) P. Guo, L. Zhang, M. A. Liu, *Adv. Mater.* **2006**, *18*, 177-180; b) N. Kurita, S. Tanaka, S. Itoh, *J. Phys. Chem. A* **2000**, *104*, 8114-8120; c) G. Iftime, F. L. Labarthet, A. Natansohn, P. Rochon, *J. Am. Chem. Soc.* **2000**, *122*, 12646-12650; d) C. Wang, Z. Wang, X. Zhang, *Accounts. Chem. Res.* **2012**, *45*, 608-618; e) X. Zhang, H. Zhao, Y. Gao, J. Tong, L. Shan, Y. Chen, S. Zhang, A. Qin, J. Z. Sun, B. Z. Tang, *Polymer* **2011**, *52*, 5290-5301; f) Y. Zhang, P. Chen, M. Liu, *Langmuir* **2006**, *22*, 10246-10250.

10.1002/chem.201800307

FULL PAPER

The mesostructure has been tuned from disordered hierarchical arrangement into an ordered 2D square *p*4*mm* structure by changing the length of alkyl chain between diquaternary ammonium head group and azobenzene group. Visible evidence for the mesostructural transformation from short range hexagonal or lamellar ordering to 2D square mesostructure is shown.

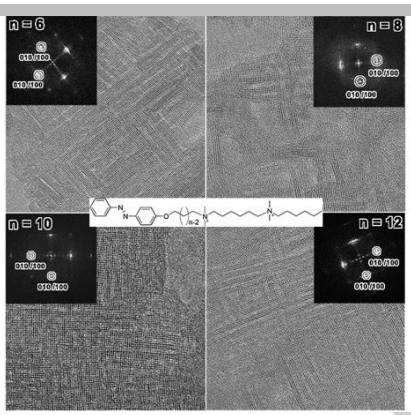

Xuefeng Shen, Wenting Mao, Yanhang Ma, Honggen Peng, Dongdong Xu, Peng Wu, Lu Han and Shunai Che**

Page No. – Page No.

Mesoporous MFI Zeolite with Two-Dimensional Square Structure Directed by Surfactants with Azobenzene Tail Group